Bidirectional Leaky-Wave Antenna Based on Dielectric Image Line for Remote Vital Sign Detection at mm-Wave Frequencies

Mingle, Solomon; Kampouridou, Despoina; Feresidis, Alexandros

DOI:
10.1109/OJAP.2022.3201630

Citation for published version (Harvard):
Mingle, S, Kampouridou, D & Feresidis, A 2022, 'Bidirectional Leaky-Wave Antenna Based on Dielectric Image Line for Remote Vital Sign Detection at mm-Wave Frequencies', *IEEE Open Journal of Antennas and Propagation*, vol. 3, pp. 1003-1012. https://doi.org/10.1109/OJAP.2022.3201630

Received 10 July 2022; revised 15 August 2022; accepted 17 August 2022. Date of publication 25 August 2022; date of current version 7 September 2022.
Digital Object Identifier 10.1109/OJAP.2022.3201630

Bidirectional Leaky-Wave Antenna Based on Dielectric Image Line for Remote Vital Sign Detection at mm-Wave Frequencies

SOLOMON MINGLE, DESPOINA KAMPOURIDOU (Member, IEEE), AND ALEXANDROS FERESIDIS (Senior Member, IEEE)

Department of Electronic/Electrical and System Engineering, University of Birmingham, Birmingham B15 2TT, U.K.
CORRESPONDING AUTHOR: S. MINGLE (e-mail: solomonmingle@gmail.com)

ABSTRACT A bidirectional leaky wave antenna (LWA) with beam scanning capabilities was developed based on the dielectric image line for single-tone continuous-wave Doppler radar (DR) for remote vital sign monitoring (RVSM) in a dynamic environment. It consists of a conductor-backed copper dielectric image line with two of the same dielectric layers mounted on top of each other for performance improvement. A RO6010 substrate with high permeability is used for the top two layers. The bottom layer is a RT/duroid 5880 low permittivity substrate stacked on top of the copper DIL to prevent higher order modes from being excited in the DIL channel. The dominant mode of the DIL is perturbed by making holes periodically in the DIL, and fast-wave space harmonics are generated. The scanning range of the proposed antenna through the broadside is 70.19°(−42.49° to 27.7°) with an impedance bandwidth of 15 GHz (50-65 GHz), an optimum gain in the fast wave area ranging from 15.5 dBi to 19.79 dBi and an efficiency of 83.8% at 57.5 GHz. Detailed RVSM tests have been performed with the proposed antenna system. It is shown that by adjusting the operating frequency from 50 GHz to 65 GHz, multiple targets' breathing rates (BR) and heart rates (HR) can be detected within 70° of the angular range.

INDEX TERMS Dielectric image line (DIL), doppler radar sensors, frequency scanning, leaky wave antenna, remote vital sign monitoring.

I. INTRODUCTION

THE USE of Doppler radar (DR) to remotely monitor vital signs such as respiratory rate and heart rate is a more convenient means of monitoring a person's vital signs than traditional invasive or contact-based vital sign monitoring systems. The amplitude and frequency of chest vibrations triggered by breathing and heartbeat are detected by a Doppler radar-based health monitoring sensor [1]. Because the amplitude of chest vibrations caused by heartbeat is so small (0.2 mm), accurate detection of respiration and heart rate is impossible with the DR, which operates in common lower microwave frequency ranges such as 2.4 GHz, 5.7 GHz, and 10 GHz [2], [3], [4], [5], [6]. Therefore, millimetre wave frequencies (50 GHz–65 GHz) are recommended to improve the performance of heart and respiratory rate detection because the shorter wavelength provides higher sensitivity [7]. Remote vital signs monitoring (RVSM) has been proposed for use in a number of domains, including routine healthcare diagnostics, emergency services, security, and military applications [1], [2], [3], [4], [5], [6], [8], [9], [10], [11]. However, before RVSM data can be used in practise, its accuracy and consistency must be adequately addressed, especially when a patient is subject to random motion [7]. To meet the criteria of these systems, planar antennas must be broadband, high-gain, low-profile, lightweight, and simple to incorporate into other technologies [12].

Leaky-wave antennas (LWAs) are interesting candidates for frequency-scanning radio systems due to their simple feed structure, high gain, and broadband performance [13]. A feature of the LWA is its ability to perform a back-to-back frequency sweep. According to [14], a dual-band

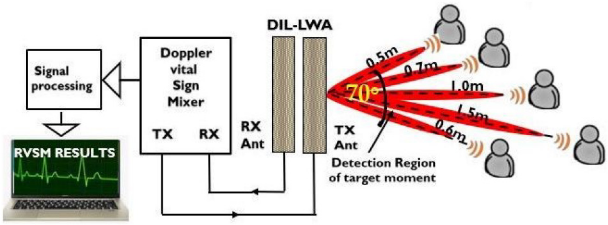

FIGURE 1. **Application scenario of the bidirectional RVSM for monitoring target through broadside.**

LWA performance at 60 GHz is achieved by a dielectric supercell grating (two different grating layers with different dimensions). The dual beam is generated by two spatial harmonics with $n = -1$ and $n = -2$ and radiates in opposite directions. In [15], a LWA for the W-band is fabricated using rectangular dielectric gratings on both sides of a dielectric image line (DIL) on a single substrate.

The advantages of DIL-based antennas include frequency scanning, low-loss performance, easy mounting and integration with other technologies. In [16], an antenna array fed through a hole in the ground plane is presented as DIL, while in [17], [18] a LWA based on an internal dielectric waveguide is proposed to operate in the frequency range of 50-85 GHz. DIL antennas are also available at the sub-THz frequency spectrum [19]. Since a DIL is a semi-open structure, power losses occur and the radiation can be controlled to meet the requirements of specific applications [18]. LWAs with dielectric gratings usually do not radiate in the exact direction of the broadside frequency because internal resonance prevents radiation there, which is called the open-stopband (OSB) phenomenon [20], [21]. These LWAs also suffer from the complexity of their fabrication due to the different types of dielectric grids [22], [23]. As far as the authors are aware, there is relatively little work on radiation-controlled antenna designs at mm-wave frequencies for health monitoring applications based on DIL, probably due to the operating frequency limit of commercially available electronic components. Recently, a preliminary work on frequency scanning aspects of leaky wave antennas (LWA) based on DIL was published [24].

In this paper, we propose a high-gain LWA based on DIL with a wideband frequency scan from 50 GHz to 65 GHz, no dielectric grating, no open-stopband, and can be fabricated at low cost. The required antenna radiation performance is calculated for RVSM through broadside in a typical case where the target is sitting down on a chair and is expected to change positions left, right, and centre as shown in Fig. 1. In the proposed antenna, a periodic array of small metallic square patches (0.6 mm x 0.57 mm x 1 mm) is employed between the dielectric layers, resulting in a high-efficiency radiator with a broadside OSB mitigation property. The proposed antenna is lightweight and does not require complex prototyping compared to other LWAs in the literature. The proposed antenna has adequate half-power beamwidth (HPBW) and beam scanning range of $70.1^\circ(-42.4^\circ$ to $+27.7^\circ)$ for noncontact vital sign detection for two or more targets at a distance up to 1.5 m with a varying gain from 15.7 dBi to 19.79 dBi in the E-plane. In our design, 42 cylindrical holes each with a diameter of 1 mm were used to achieve broadside radiation at about 57.5 GHz at reasonable radiation quality and to stay within the limits of available fabrication equipment. To the best of our knowledge, this is the first non-contact vital sign radar sensor to use dielectric image line leaky wave antennas.

This paper is organized as follows: Section II describes the full leaky wave antenna design, Section III presents the antenna measurement results and discussions, Section IV deals with health monitoring measurements and finally, Section V concludes the work.

II. LEAKY WAVE ANTENNA DESIGN

We first demonstrate the unit cell analysis and design methodology, according to the theory of leaky waves. Next, we present details of the finite size leaky-wave antenna, as well as its feeding network.

A. DIL UNIT CELL ANALYSIS AND DESIGN

The proposed unit cell of the DIL antenna is presented in Figure 2(a). It is characterized by a number of design parameters, where $2a$ represents the DIL's width, b represents the substrate thickness, p represents the perturbation period, and d represents the hole's diameter on Rogers RT/duroid6010LM (tm) substrate ($\epsilon_r = 10.7, tan\delta = 0.0023$). The substrate is chosen with a reasonably high dielectric constant, so that it allows the fields to the DIL to remain intact and it reduces radiation leakage via the DIL.

Having decided on the substrate, we need to decide on the thickness and width of the DIL. Since not all substrate thicknesses are commercially available, we first selected the appropriate DIL thickness and then, to keep the field confinement and whether the DIL operates in single-mode or multimode, can be determined by α/λ_0 where λ_0 is the free space wavelength at the design frequency, which determines field confinement and whether the DIL is single-mode or multimode. Single-mode operation and excellent field confinement are computed for unity aspect ratio ($b = a$) as [25]:

$$\frac{\alpha}{\lambda_0} \approx \frac{0.32}{\sqrt{\epsilon_r - 1}} \tag{1}$$

The estimated value of a is 0.54 mm, equal to the calculated value of b using the unit aspect ratio and eq. (1) at the centre frequency of V-band (57.5 GHz). The nearest commercially available thickness of 0.62 mm is taken in our design and the width ($2a = 1.08$ mm) is selected accordingly. The optimized dimensions of the unit cell can be viewed in Table 1.

The unit cell can now be analyzed using leaky-wave theory, which provides useful guidelines for high gain and broadband antenna performance. It simplifies the analysis of large arrays by assuming that the array is infinite, that the patterns of the individual elements are similar, and that the array is uniformly excited in amplitude but not necessarily

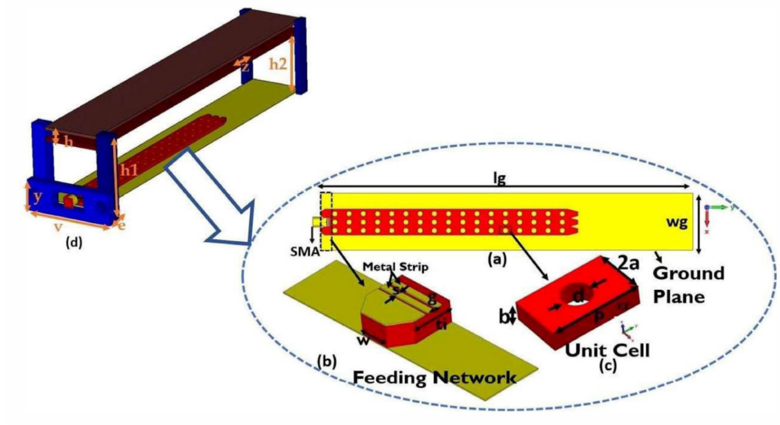

FIGURE 2. Schematic of (a) DIL antenna, (b) unit cell, (c) feeding network, (d) full proposed antenna.

TABLE 1. Dimensions of the proposed antenna of Fig. 2.

Parameter	Value [mm]	Parameter	Value [mm]
v	10.9	2a	1.6
z	4.8	b	0.6
h	0.9	p	2.7
h_1	6.3	d	1
h_2	5.13	w	0.6
y	4.03	ti	0.9
e	2	g	0.09
Lg	61.2	s	0.18
wg	7.1		

in phase. This creates a clear design guideline and simplifies the superposition equation of Bloch-Floquet theory, which states that periodic structures can support an infinite number of spatial harmonics as [13]:

$$\beta_n = \beta_0 + 2\pi n/p \tag{2}$$

where β_0 and β_n are the propagation constants for the fundamental and n-th order space harmonics, respectively, p is the period and n is an integer. In general, the fundamental space harmonic is a slow wave, but the $n = -1$ space harmonic is fast and radiates in free space.

It is well-known that fast waves are necessary for the generation of leaky waves. In the present structure, fast spatial harmonics are formed by periodic perturbations of cylindrical holes along the axial line of the fundamental structure. The radiation direction of the fundamental beam in the periodic LWA for $n = -1$ space harmonic is calculated as follows:

$$\theta = \sin^{-1}\left(\frac{\beta_0(\omega)}{k_0} - \frac{2\pi}{k_0 \times p}\right) \tag{3}$$

where θ is the angle measured from the z-axis (Fig. 2) and k_0 is the free-space wavenumber.

Using eq. (3), we can make an initial estimate of the period p for a given main beam direction and frequency. We aim for broadside ($\theta = 0$) radiation of the main beam at 57.5 GHz. A full-wave dispersion analysis of the unit cell under consideration is provided. The study was performed using a robust tool first presented in [26], which has been successfully applied to numerous leaky wave antennas [27], [28].

For the full-wave simulation of the unit cell of Fig. 2(c) with CST Microwave Studio, the computational domain is defined as follows: periodic boundaries along x and y axes, PEC at $-z$ axis, and open space at $+z$ axis. Since the propagation of the leakage mode occurs along $+y$ axis, a phase shift ξ is introduced from the negative to the positive boundaries. The unit cell is excited with a very small dipole source within its domain. For the calculation of the phase constant β, the maximum of the electric field component E_y at resonant frequencies f_r is then followed, which depends on the phase shift ξ, according to:

$$\beta = k_0\,(f_r)\,p \tag{4}$$

The phase shift ξ is scanned from 0° to 180°. A setup of two-unit cells is used to calculate the attenuation constant. The maxima of the E-field components at two measurement points are separated by one period p. The exponential decay of the electric fields between these two sampling points is a measure of the attenuation constant α of the leaky mode:

$$\alpha = -\frac{1}{p}\ln\frac{E_1}{E_0} \tag{5}$$

where E_0 is the electric field (in V/m) at the source-fed unit cell and E_1 is the E-field at the next unit cell at a distance p.

The aforementioned method is applied for the unit cell of dimensions as shown in Fig. 2(c) and Table 1. The wavenumber of the leaky mode is presented in Fig. 3. For an infinitely long unidirectionally fed DIL antenna, broadside radiation is expected around 57.5 GHz (where $\beta = 0$). The main beam scans from the rear quadrant (below 57.5 GHz) to the front quadrant (after 57.5 GHz). At 57.5 GHz, where $\beta = 0$, it is $\alpha > 0$, suggesting elimination of the open-stopband. A small variation in the calculated parameters, such as the frequency of close-to-broadside radiation, is to be expected since the finite-size model will not reach infinity. Recall that for 90% power transmission, the antenna length L should be $0.18\lambda_0/\alpha$ [13].

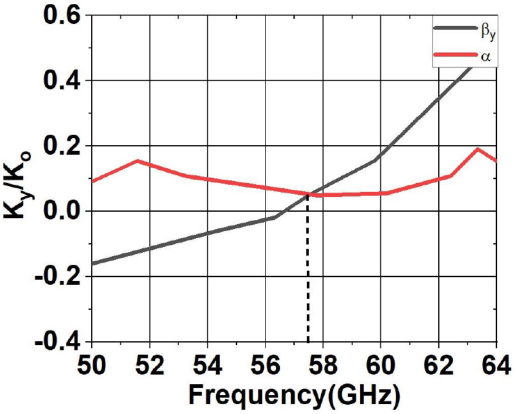

FIGURE 3. Calculated wavenumber of the leaky mode of the DIL unit cell.

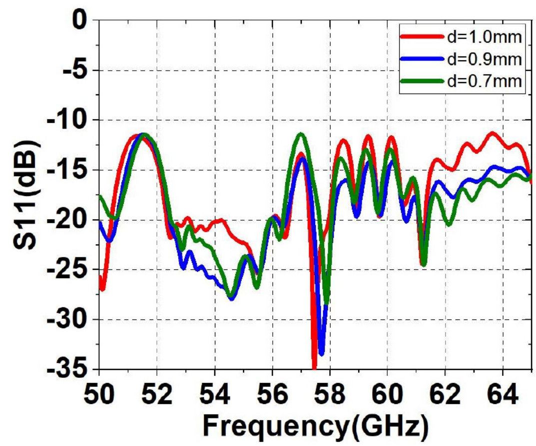

FIGURE 4. S_{11} parameters variation of the full proposed antenna with respect to d.

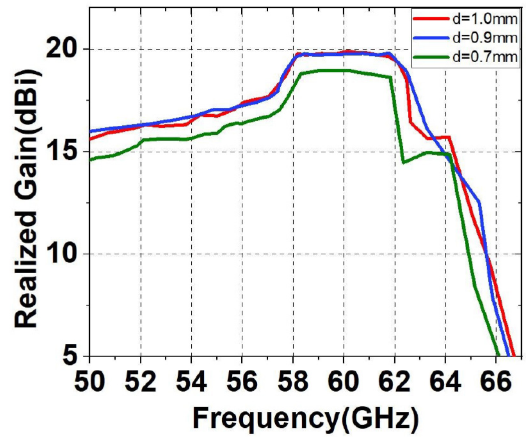

FIGURE 5. Realized gain variation of the full proposed antenna with respect to d.

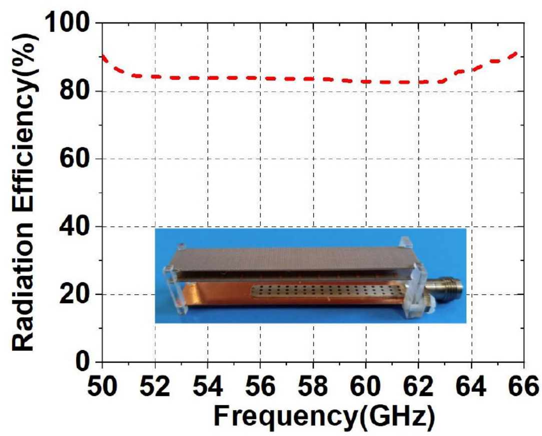

FIGURE 6. Simulated radiation efficiency of the proposed antenna.

B. FEEDING NETWORK

The proposed feeding network for the finite size DIL is shown in Fig. 2(b), which is a planar substrate truncated microstrip line-to-DIL, with two extra metal strips that is substrate-truncated. Based on generalised empirical equations presented in [23] for the chosen substrate and frequency band, the length of the tapered microstrip line (ti) and metal strip width (s) with inter-element gap (g) were optimized. The optimized dimensions are available in Table 1.

C. FULL PROPOSED ANTENNA

The full-proposed leaky-wave antenna can be viewed in Fig. 2(a). The finite size DIL consists of 3×17 unit cells in x and y axes accordingly. The overall size of this antenna is $L_g \times wg = 61.2 \times 7.1$ mm^2, so that acceptable radiation quality is achieved while staying within the limits imposed by available fabrication capabilities. To further boost the gain and efficiency of the proposed antenna, two dielectric plates of Taconic TLY-5 (lossy) substrate with the same thickness $t = 0.508$ mm were placed above the DIL at a spaced height ($h_1 = 6.34$ mm and $h_2 = 0.62$ mm) between the ground plane and the first and second dielectric plates, respectively.

III. SIMULATION RESULTS

Figure 4 shows the simulated S_{11} parameters of the proposed antenna with small optimization of the different hole sizes d. The S_{11} parameters are below -10 dB from 50 GHz to 68 GHz. The variation of the realized gain with different hole diameters d is shown in Fig. 5. The maximum gain of the simulated finite-size antenna is stable between 58 and 62 GHz at 19.9 dBi. It can be seen that a constant gain is achieved at 58 GHz to 63 GHz, where open-stopband is suppressed. It is evident that the selection of the hole diameter $d = 1$ mm is the optimum, as it leads to higher realized gain.

The proposed antenna can radiate a fan beam with continuous beam scanning in the yz plane. The main beam is directed to the broadside 57.5 GHz, which corresponds to the unit cell dispersion curve shown in Figure 3. In Fig. 6 the radiation efficiency of the antenna is depicted, which remains over 80% within all the frequency range of interest. At the 57.5 GHz, where radiation at broadside is achieved, this value is 83.8%. The simulated results of the antenna are close to the expected values, as shown in the last paragraph.

The simulated 2D and 3D radiation patterns in the E-plane are shown in Fig. 7. The simulated range of the main beam

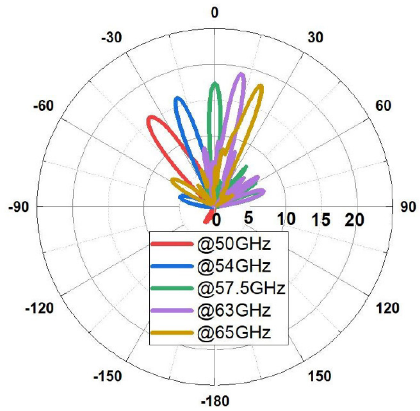

(a)

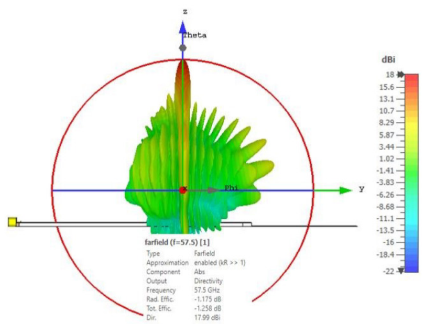

(b)

FIGURE 7. ***E*-plane of (a) 2-D radiation pattern at several frequencies and (b) 3-D radiation pattern of the proposed antenna at 57.5 GHz.**

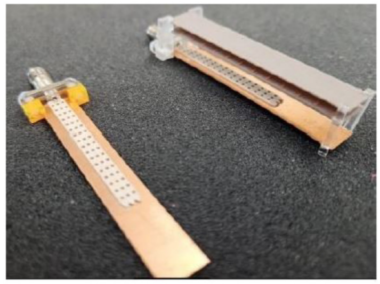

FIGURE 8. Photo of dielectric image line LWA with and without extra plain dielectric layers.

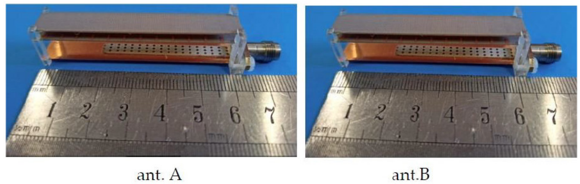

FIGURE 9. Manufactured LWA prototype for RVSM where ant. A is for transmitting and ant. B for receiving.

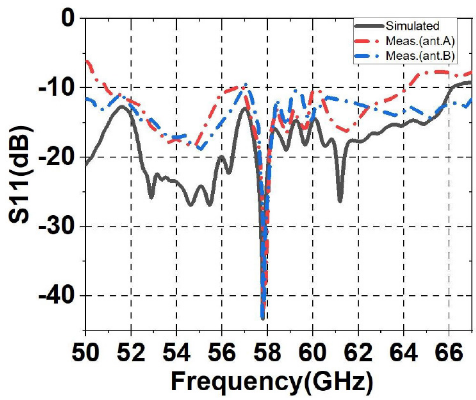

FIGURE 10. Measured and simulated S_{11}-parameters.

scanning is 70.19° (−42.49° to 27.7°) with only 3 dB scanning loss, which is consistent with the dispersion analysis of the previous Section. The sidelobe level remains below −10 dB in all cases. It should be noted that the backward and forward scanning of the beam is not symmetrical. The forward scan range can be improved by maintaining the position of the backward beam if the impedance matching can be improved up to 68 GHz (range of fast single beam waves).

IV. MEASURED ANTENNA RESULTS AND DISCUSSION

The antenna structure, including the coaxial feed, is housed in a low-loss polytetrafluoroethylene (PTFE) enclosure that allows practical mounting and measurement of the antenna. In addition, a tiny piece of the PTFE plastic was used as a spacer to keep the boards parallel and at the required height above the ground plane and not interfere with the antenna's radiation. A photo of the antenna prototype with and without additional dielectric layers is shown in Fig. 8. It should be noted here that the proposed antenna with an additional dielectric plate was used for the RVSM because of its high gain and beam scanning performance.

The resonance distance of the first and second dielectric layers from the ground plane was established with spacers of 5.13 mm and 0.9 mm, respectively. The tolerance in the distances was ś 0.05 mm due to the tolerance of the spacers and the material used for the housing of the antenna. A 1.85 mm flanged launcher with a GB185 glass bead is used for the connection to the outside world. A common, low-cost PCB fabrication technique was used to produce the antenna layers. Fig. 9 shows two copies of the LWA prototype built for RVSM (antenna A and antenna B). Fig. 10 shows a very high agreement between the calculated and measured S_{11} response of the proposed DIL LWA, while Fig. 11(a) demonstrates a comparison of the modelled and measured far-field radiation pattern (FRP) of the *E*-plane with an excellent radiation pattern result. In detail, the levels of co-polar and cross-polar can be seen for *E*- and *H*- plane at the frequency of broadside (57.5 GHz). The cross-polar level remains satisfactory at both planes, with excellent agreement between simulations and measurements. Similar cross-polar level can be expected for other frequencies. Table 2 summarises the results of the two antennas for the RVSM application. Figure 12 also shows significant agreement between the simulated and measured gain response.

Table 3 shows the proposed LWA compared to similar published studies. The proposed antenna has a short length,

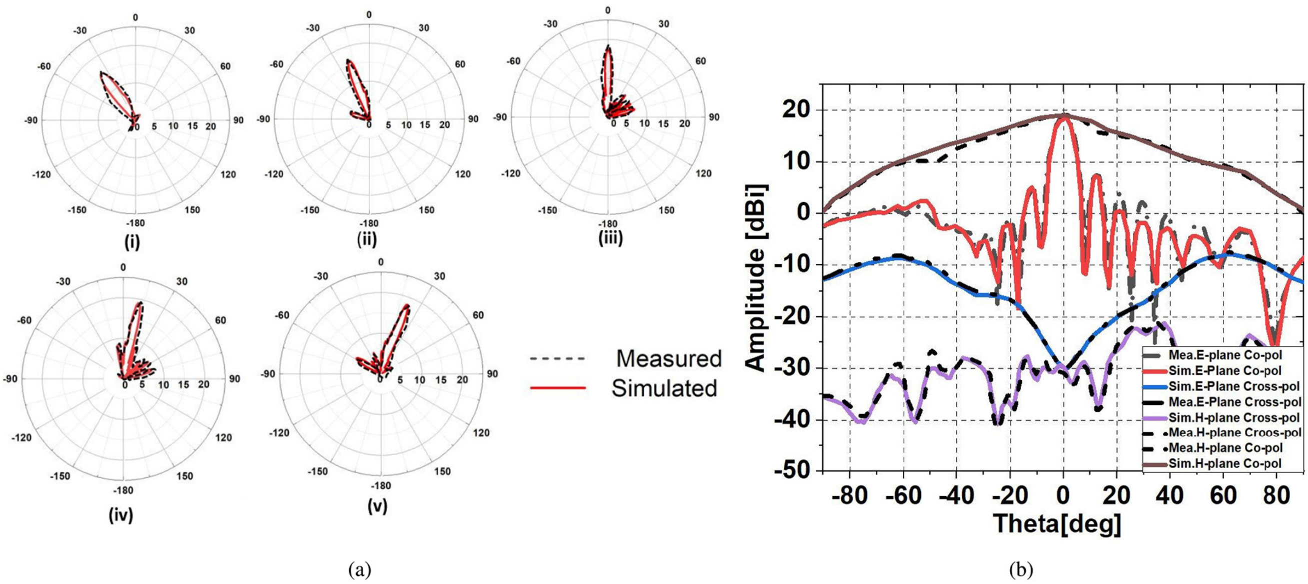

FIGURE 11. (a) Measured and simulated FRPs in *E*-plane of the proposed antenna at (i) 50 GHz, (ii) 54 GHz, (iii) 57.5 GHz, (iv) 63 GHz, and (v) 65 GHz. (b) Measured and simulated copolar and crosspolar at *E*- and *H*-planes at 57.5 GHz.

TABLE 2. Measured antennas' performances.

	Ant. A	Ant. B	Simulated
BW ($S_{11} < -10\,dB$)	50 - 64 GHz	50 - 66 GHz	50 - 67 GHz
Max. Gain (dBi)	19.7 @63 GHz	19.8 @ 63 GHz	18.5 @ 57.5 GHz
Scanning Range (50 - 65 GHz)	-42^o to +27^o	-43^o to $+26.3^o$	-47^o to $+23^o$
HPBW Variation	12^o - 5^o	14^o - 7^o	9^o - 6^o

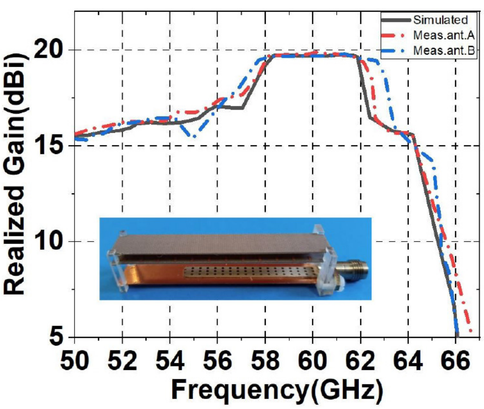

FIGURE 12. Measured and simulated realized gain of the proposed antenna.

relatively high gain, and provides a wider beam scanning radiating from back to front. Compared to other similar antennas in the literature, our proposed design exhibited a suitable configuration that operates as a LWA with superior characteristics at millimetre-wave frequencies. Although most antennas in the literature can scan to the broadside, compared to all other antennas with some degree of complexity in the literature, our proposed antenna has a wider scanning range with lower

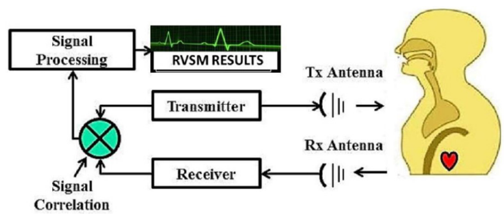

FIGURE 13. Demonstration of the RVSM experiment setup measurements.

fabrication cost. For example, there were slight differences between the simulated and observed results in [14] and [15] due to the inherent air gap between the ground plane and the dielectric layer during fabrication, so the radiation on the broadside was not considered.

V. MEASUREMENTS OF REMOTE VITAL SIGNALS WITH DOPPLER RADAR RESULTS AND DISCUSSION

Figure 13 illustrates the steps involved in remote vital sign monitoring (RVSM) when Doppler radar technology is used to detect vital signs. A continuous EM tone at a single frequency is transmitted via a transmitting antenna (Tx). The wave is reflected at a distance m from the subject's chest and picked up by a receiver antenna (Rx). The quasi-periodic vibration of the chest caused by breathing and heartbeat is phase modulated by the received signal. The phase modulated signal is demodulated at the receiver (Rx) and correlated with the transmitted signal, and the resulting data is stored for a period of time. To extract the person's breathing and heartbeat, the raw data is processed in the time domain using various signal processing techniques such as digital filtering and Fourier transform.

According to the Doppler radar theory, for a transmitted signal $S(t) = cos(2\pi ft + \phi(t))$, where f and $\phi(t)$ are the frequency and phase of the transmitted wave, respectively,

TABLE 3. Comparison of the proposed LWA with recently reported DIL LWAs.

	[14]	[15]	[16]	[17]	[18]	**This work**
Freq.(GHz)	57-63	97-103	8-12	50-85	9-14	**50-66**
Number of beams	Dual $(n=-1, n=-2)$	Single $(n=-1)$	Single $(n=-1)$	Single $(n=-1)$	Single $(n=-1)$	**Single** $(n=-1)$
Radiation at $\theta = 0^o$	No	No	Yes	Yes	Yes	**Yes**
Scanning range	-30^o to -20^o	-20^o to -2^o	-35^o to $+35^o$	-9^o to $+40^o$	-40^o to $+35^o$	-42.29^o **to** $+27.7^o$
Gain (dBi)	23	18	10.5 to 12.5	9.1 to 14.2	8 to 13	**15 to 19**
BW%	10	6	40	58	41.6	**25.6**
Length of antenna	$58\lambda_0$ @ 60 GHz	$5\lambda_0$ @ 100 GHz	NA	$8\lambda_0$ @ 60 GHz	$6\lambda_0$ @ 12 GHz	**$11\lambda_0$ @ 57.5 GHz**

the received baseband signal $R(t)$ may be approximated as [29]:

$$R(t) = cos[\theta(t) + \frac{4\pi x_b(t)}{\lambda} + \frac{4\pi x_h(t)}{\lambda}] \tag{6}$$

where θ_t is the total phase shift due to the signal path (d), reflections from the subject and surroundings and residual phase noise, λ, $x_b(t)$ and $x_h(t)$ are the operating wavelength, and chest vibration signals due to respiration and heartbeat, respectively. Due to the periodic nature of the $x_b(t)$ and $x_h(t)$ they may be approximated as: $x_b(t) = m_b sin(2\pi f_b t)$ and $x_h(t) = m_h sin(2\pi f_h t)$, where m_b and m_h are the displacement amplitudes of the chest motion due to respiration and heartbeat, respectively, f_b and f_h are the frequencies of BR and HR, respectively. This way, the expansion of equation (6) in the Fourier series leads to [30]:

$$R(t) = \sum_{i=-\infty}^{\infty} \sum_{j=-\infty}^{\infty} J_j[\frac{4\pi m_b}{\lambda}] J_i[\frac{4\pi m_h}{\lambda}] \times cos(j2\pi f_b t + i2\pi f_h t + \theta) \tag{7}$$

where $J_n(X)$ Bessel function of the first kind with argument X. Taking the first positive harmonics of both f_b and f_h into account the above equation can be written as:

$$R(t) = J_1[\frac{4\pi m_b}{\lambda}] J_0[\frac{4\pi m_h}{\lambda}] cos(2\pi f_b t + \theta) + J_0[\frac{4\pi m_b}{\lambda}] J_1[\frac{4\pi m_h}{\lambda}] cos(2\pi f_h t + \theta) \tag{8}$$

where $J_1[\frac{4\pi m_b}{\lambda}] J_0[\frac{4\pi m_h}{\lambda}]$ and $J_0[\frac{4\pi m_b}{\lambda}] J_1[\frac{4\pi m_h}{\lambda}]$ are the amplitudes of the phase variations in $R(t)$ due to respiration and heartbeat, respectively. Equation (9) contains the essential information related to the applicability of mm-wave frequencies for RVSM. Based on equation (9), we analyse and visualise the main factors involved in the RVSM steps and experimental setup (see Fig. 14(a)).

An extensive series of measurements were performed to verify the efficiency of the prepared scanning antennas and to determine the vitality of the antennas from a fixed location. The VNA is calibrated at 0 dBm for transmission (Tx) and reception (Rx) of electromagnetic (EM) waves in the range of 50-66 GHz for the gain of 201 points.

As can be seen in Fig. 14(b), the subject sits in front of the antennas at various radial distances or angular positions. For 60 seconds (the collection time, equal to the duration of each

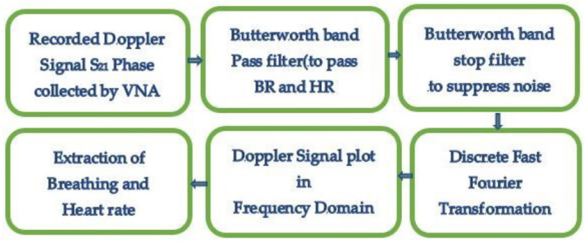

(a)

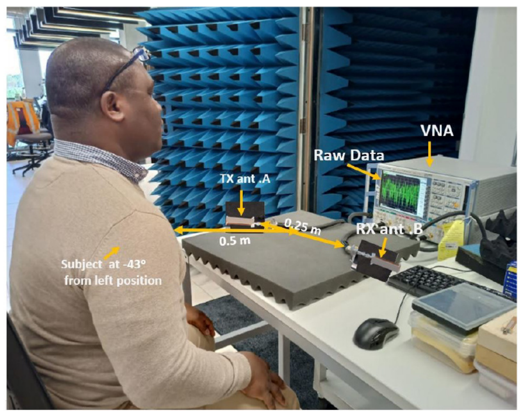

(b)

FIGURE 14. (a) RVSM digital signal processing steps. (b) Experiment setup.

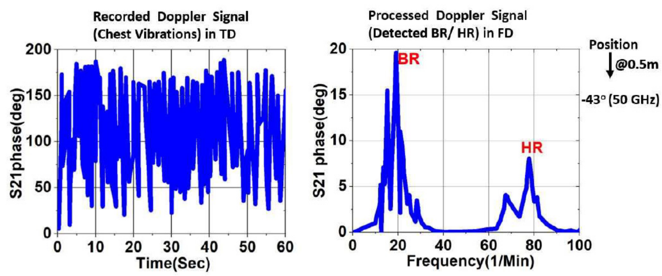

FIGURE 15. Measured RVSM results from 0.5 m distance at 50 GHz (LWA main beam at −43° with 6° HPBW).

data set), a continuous wave (CW) time sweep is performed with a single tone. During the sweep, the Tx antenna in port 1 of the VNA transmits and the Rx antenna on port 2 of the VNA receives the EM signal. For 60 seconds, the VNA records the phase demodulated signal as an S-parameter, i.e., S_{21} phase. Then, the recorded S_{21} phase data are acquired

TABLE 4. Measured BR and HR at different distances and angular positions.

50 GHz (-43^o)	53 GHz (-27^o)	57.5 GHz (0^o)	63 GHz ($+13^o$)	65 GHz ($+27^o$)	Manual Counter BR Contact Device HR		Max.- Min. Error
BR-HR (1/min) @0.5 m	BR-HR (1/min) @0.7 m	BR-HR (1/min) @1 m	BR-HR (1/min) @1.5 m	BR-HR (1/min) @0.6 m	BR (1/min)	HR (1/min)	BR-HR (1/min)
19-79	20-78	20-80	20-79	19-74	19-20 (avg.20)	78-81 (avg. 79)	4.8% - 1.9%

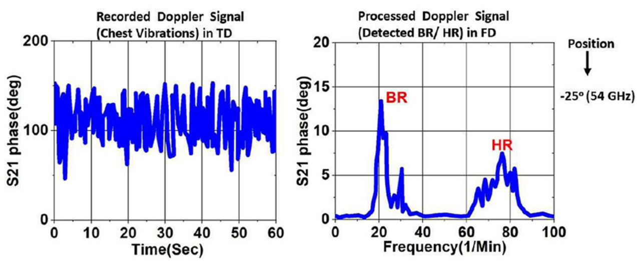

FIGURE 16. Measured RVSM results from 0.7 m distance at 54 GHz (LWA main beam at −25° with 8° HPBW).

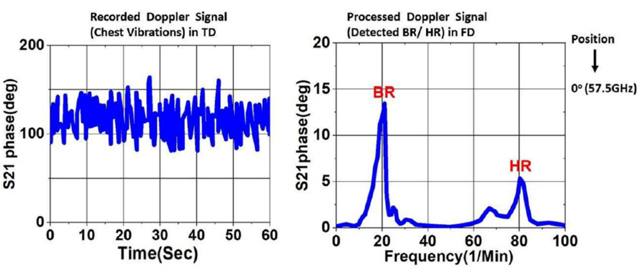

FIGURE 17. Measured RVSM results from 1 m distance at t 57.5 GHz (LWA main beam at 0° with 11° HPBW.

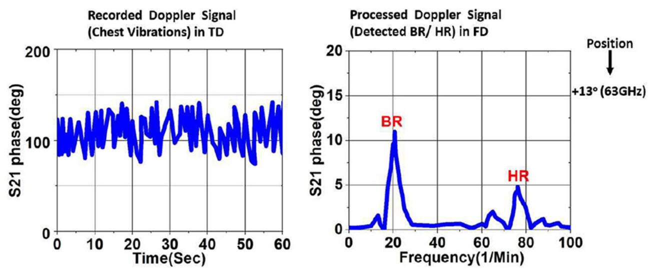

FIGURE 18. Measured RVSM results from 1.5 m distance at 63 GHz (LWA main beam at 13° with 8° HPBW).

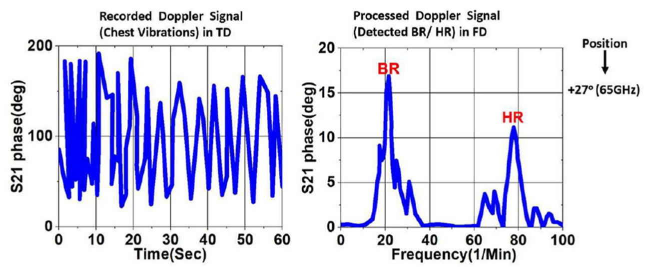

FIGURE 19. Measured RVSM results from 0.7 m distance at 65 GHz (LWA main beam at 27° with 5° HPBW).

by a laptop and analyzed by a signal processing application in MATLAB to extract the values for necessary respiration (BR) and heart rate (HR). The signal processing software mainly consists of discrete fast Fourier transform (DFFT) to convert the time domain signal (TD) to the frequency domain (FD), bandpass filters to pass the frequencies BR and HR, and bandstop filters (tenth-order Butterworth digital filters) for noise reduction, data readout, and display. Because we are only interested in the average BR and HR (1/min) results in FD (not BR and HR waveforms in time) to justify the possibility of RVSM detection in the context of the proposed antenna beam steering, no electrocardiogram (ECG) is used for waveform comparison in the presented beam scanning DR. Previous studies have used ECG and fingertip pulse oximeter sensors to demonstrate specific waveform detection accuracy, time domain (TD), BR, and HR with DR [31].

The digital signal processing techniques used here (DSP) were used for noise reduction and the extraction of respiration and heart rate from the signals obtained with the VNA. The first step was to separate the heart and respiratory signals. To accomplish this, the signal obtained from the VNA was first passed through the cutoff frequencies of a 10th order Butterworth bandpass filter based on the expected BR (1/min) of 10 GHz–41 GHz, and it was passed through an 8th order Butterworth bandstop filter for the expected minimum heart rate/min of 61 to the maximum cutoff heart rate of 98. The order of the filters was chosen considering the most accurate results from the analysis of the collected data [32]. After filtering, the heart rate and respiration rate were calculated over a time window of a few seconds using a discrete fast Fourier transform (DFFT), which then determined the BR and HR. Cutoff values were chosen based on the average maximum and minimum heart rate and respiratory rate.

For experimental demonstration of the designed vital sign radar system, the transmit and receive ports of the radar system measurement setup shown in Figure 14 are connected to the scan antennas shown in Figure 9. Since the broadside direction of the antenna is specified as 0°, the human targets remain stationary and are located in front of the Tx/Rx antennas at distances of 0.5 m, 0.7 m, 1 m, 1.5 m, and 0.6 m, corresponding to five different angular positions: $-43°, -25°, 0°, +13°$ and $+27°$. The S_{21} phase data (demodulated Doppler signal in TD) are acquired at 50 GHz, 54 GHz, 57.5 GHz, 63 GHz and 65 GHz for each

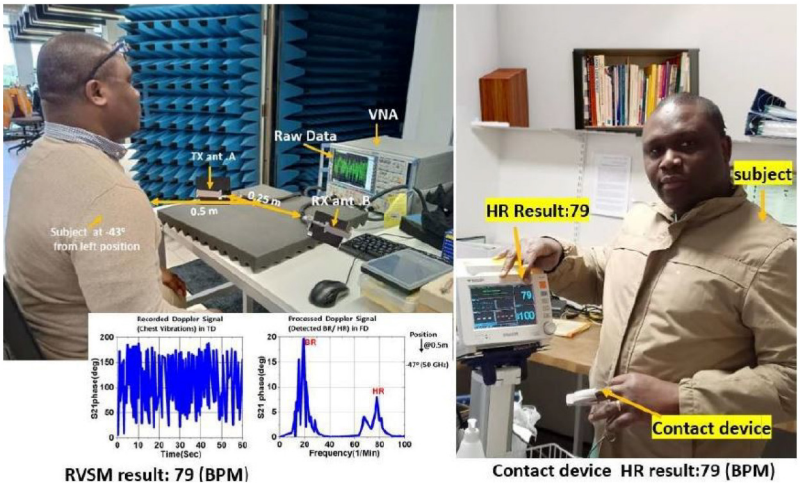

FIGURE 20. Validation of the measured heart rate results compared with the traditional method.

angular point respectively. Consequently, we obtain five sets of S_{21} phase data for 50 GHz, 54 GHz, 57.5 GHz, 63 GHz and 65 GHz at the desired five angular points, as shown in Figures 15–19. The depicted phase in these Figures is the direct phase, which is the same with the raw data.

The left column (LHS) of each image shows the recorded Doppler signal in TD, while the right column (RHS) shows the matching processed signal in FD. The first peak at a frequency of about 20 (1/min) represents the expected amplitude of the BR signal, while the second peak at a frequency of about 80 (1/min) represents the expected amplitude of the HR signal. Both the measured BR and HR signals had sufficiently larger amplitudes than the resulting noise levels for the subject locations at low angles. These results are consistent with expectations; at 57.5 GHz, the antenna radiation beam is centered at about 0° with more than 12° HPBW [see Fig. 11(a)(iii) and Table 2]. Figs. 15–19 show that the recorded Doppler signal with the largest amplitude compared to the surrounding noise levels is recorded for measurements with higher angles for high-frequency signals. This is especially true for the tiny HR peak, which is more susceptible to noise trapping.

Table 4 shows all the measurements for BR and HR of a single target at different angular locations and distances. To validate the proposed design concept, a traditional blood pressure machine, demonstrated in Fig. 20, has been used to take the heart rate of the same subject and an average of the results agrees with the non-contact radar approach.

It can be inferred that the RVSM detection response of the proposed antenna has the potential to track both single and multiple targets' vital signs over an angular range of $-43°$ to $27°$ up to 1.5 m, which corresponds to an angular range of 70° (see Fig. 1 when scanning the operating frequency of 50 GHz to 65 GHz). Since the antenna gain and transmit power are sufficient, there is a possibility to use this antenna for RVSM with a range of more than 2 m. A small error for BR and HR was found due to the inaccuracy of the calibration of the VNA and the wear of the cables.

VI. CONCLUSION

A bidirectional LWA with high gain, high efficiency, and frequency scanning is preferable to a static antenna design for RVSM with one or more targets in situations where the object is moving at different angles. The antenna is fabricated using common, low-cost PCB fabrication techniques and operates in the mm-waveband to take advantage of open-band licensing and minimal noise. Two copies of the proposed antenna were fabricated, described, and tested. The measured and simulated results agree well, and the antennas have been successfully used to detect respiration and heartbeat at radial distances between 0.5 and 1.5 metres and at angular positions between $-43°$ and $+27°$ to the subject's body. In addition, the design method could be particularly useful for producing low-cost, high-gain, longer-range antennas at even higher mm-wave frequencies.

REFERENCES

[1] D. Obeid, G. Zaharia, S. Sadek, and G. El Zein, "Microwave doppler radar for heartbeat detection vs electrocardiogram," *Microw. Opt. Technol. Lett.*, vol. 54, no. 11, pp. 2610–2617, 2012.

[2] A. D. Droitcour *et al.*, "Non-contact respiratory rate measurement validation for hospitalized patients," in *Proc. 31st Annu. Int. Conf. IEEE Eng. Med. Biol. Soc. Eng. Future Biomed.*, 2009, pp. 4812–4815.

[3] M. S. Rabbani and H. Ghafouri-Shiraz, "Ultra-wide patch antenna array design at 60ăGHz band for remote vital sign monitoring with doppler radar principle," *J. Infrared, Millimeter, Terahertz Waves*, vol. 38, no. 5, pp. 548–566, 2017.

[4] M. Villarroel *et al.*, "Continuous non-contact vital sign monitoring in neonatal intensive care unit," *Healthcare Technol. Lett.*, vol. 1, no. 3, pp. 87–91, 2014.

[5] M. S. Rabbani and H. Ghafouri-Shiraz, "Accurate remote vital sign monitoring with 10ăGHz ultra-wide patch antenna array," *AEU Int. J. Electron. Commun.*, vol. 77, pp. 36–42, Jul. 2017.

[6] S. Suzuki, T. Matsui, M. Kagawa, T. Asao, and K. Kotani, "An approach to a non-contact vital sign monitoring using dual-frequency microwave radars for elderly care," *J. Biomed. Sci. Eng.*, vol. 6, no. 7, pp. 704–711, 2013.

[7] Z. Yang, P. H. Pathak, Y. Zeng, X. Liran, and P. Mohapatra, "Vital sign and sleep monitoring using millimeter wave," *ACM Trans. Sensor Netw.*, vol. 13, no. 2, p. 14, 2017.

[8] M. S. Rabbani and H. Ghafouri-Shiraz, "Frequency selective surface antenna for remote vital sign monitoring with ultra-wide band doppler radar," *Microw. Opt. Technol. Lett.*, vol. 59, no. 4, pp. 818–823, 2017.

[9] C. Gu, "Short-range noncontact sensors for healthcare and other emerging applications: A review," *Sensors*, vol. 16, no. 8, p. 1169, 2016.

[10] C. Li, V. M. Lubecke, O. Boric-Lubecke, and J. Lin, "A review on recent advances in doppler radar sensors for noncontact healthcare monitoring," *IEEE Trans. Microw. Theory Techn.*, vol. 61, no. 5, pp. 2046–2060, May 2013.

[11] M. S. Rabbani, J. Churm, and A. P. Feresidis, "Fabry-Perot beam scanning antenna for remote vital sign detection at 60 GHz," *IEEE Trans. Antennas Propag.*, vol. 69, no. 6, pp. 3115–3124, Jun. 2021.

[12] R. Agarwal, A. Agarwal, A. Dwivedi, and A. Sharma, "Leaky wave antenna for millimeter wave utilization," in *Proc. J. Phys. Conf. Ser.*, 2021, Art. no. 12026.

[13] D. R. Jackson and A. A. Oliner, "Leaky-wave antennas," in *Modern Antenna Handbook*. Hoboken, NJ, USA: Wiley, 2007.

[14] Z. L. Ma, K. B. Ng, C. H. Chan, and L. J. Jiang, "A novel supercell-based dielectric grating dual-beam leaky-wave antenna for 60-GHz applications," *IEEE Trans. Antennas Propag.*, vol. 64, no. 12, pp. 5521–5526, Dec. 2016.

[15] A. Zandieh, A. S. Abdellatif, A. Taeb, and S. Safavi-Naeini, "Low-cost and high-efficiency antenna for millimeter-wave frequency-scanning applications," *IEEE Antennas Wireless Propag. Lett.*, vol. 12, pp. 116–119, 2013.

[16] A. S. Al-Zoubi, A. A. Kishk, and A. W. Glisson, "Aperture coupled rectangular dielectric resonator antenna array fed by dielectric image guide," *IEEE Trans. Antennas Propag.*, vol. 57, no. 8, pp. 2252–2259, Aug. 2009.

[17] X. Bai, S. W. Qu, K. B. Ng, and C. H. Chan, "Sinusoidally modulated leaky-wave antenna for millimeter-wave application," *IEEE Trans. Antennas Propag.*, vol. 64, no. 3, pp. 849–855, Mar. 2016.

[18] A. Mallahzadeh and S. Mohammad-Ali-Nezhad, "Periodic collinear-slotted leaky wave antenna with open stopband elimination," *IEEE Trans. Antennas Propag.*, vol. 63, no. 12, pp. 5512–5521, Dec. 2015.

[19] Y. Torabi, G. Dadashzadeh, A. Lalbakhsh, and H. Oraizi, "High-gain and low-profile dielectric-image-line leaky-wave-antenna for wide-angle beam scanning at sub-THz frequencies," *Opt. Laser Technol.*, vol. 150, Jun. 2022, Art. no. 107968.

[20] X. Huang, Y. Lai, Z. H. Hang, H. Zheng, and C. T. Chan, "Dirac cones induced by accidental degeneracy in photonic crystals and zero-refractive-index materials," *Nat. Mater.*, vol. 10, no. 8, pp. 582–586, 2011.

[21] P. Moitra, Y. Yang, Z. Anderson, I. I. Kravchenko, D. P. Briggs, and J. Valentine, "Realization of an all-dielectric zero-index optical metamaterial," *Nat. Photon.*, vol. 7, no. 10, pp. 791–795, 2013.

[22] F. K. Schwering and S.-T. Peng, "Design of dielectric grating antennas for millimeter-wave applications," *IEEE Trans. Microw. Theory Techn.*, vol. 31, no. 2, pp. 199–209, Feb. 1983.

[23] C. S. Prasad and A. Biswas, "Dielectric image line-based leaky-wave antenna for wide range of beam scanning through broadside," *IEEE Trans. Antennas Propag.*, vol. 65, no. 8, pp. 4311–4315, Aug. 2017.

[24] S. Mingle, D. Kampouridou, and A. Feresidis, "Beam-scanning leaky-wave antenna based on dielectric image-line for millimetre-wave applications," in *Proc. 51st Eur. Microw. Conf. (EuMC)*, 2022, pp. 261–264.

[25] P. Bhartia and I. J. Bahl, *Millimeter Wave Engineering and Applications*. New York, NY, USA: Wiley, 1984.

[26] T. Kokkinos, C. D. Sarris, and G. V. Eleftheriades, "Periodic FDTD analysis of leaky-wave structures and applications to the analysis of negative-refractive-index leaky-wave antennas," *IEEE Trans. Microw. Theory Techn.*, vol. 54, no. 4, pp. 1619–1630, Jun. 2006.

[27] J. R. Kelly, T. Kokkinos, and A. P. Feresidis, "Analysis and design of sub-wavelength resonant cavity type 2-D leaky-wave antennas," *IEEE Trans. Antennas Propag.*, vol. 56, no. 9, pp. 2817–2825, Sep. 2008.

[28] D. Kampouridou and A. Feresidis, "Full-wave leaky-wave analysis of 1-D periodic corrugated metal surface antennas," *IEEE Antennas Wireless Propag. Lett.*, vol. 20, no. 5, pp. 863–867, May 2021.

[29] C. Gu, C. Li, J. Lin, J. Long, J. Huangfu, and L. Ran, "Instrument-based noncontact doppler radar vital sign detection system using heterodyne digital quadrature demodulation architecture," *IEEE Trans. Instrum. Meas.*, vol. 59, no. 6, pp. 1580–1588, Jun. 2010.

[30] C. Li and J. Lin, "Optimal carrier frequency of non-contact vital sign detectors," in *Proc. IEEE Radio Wireless Symp.*, 2007, pp. 281–284.

[31] A. Tariq and H. Ghafouri-Shiraz, "Noncontact heart rate monitoring using doppler radar and continuous wavelet transform," *Microw. Opt. Technol. Lett.*, vol. 53, no. 8, pp. 1793–1797, 2011.

[32] M. S. Rabbani, "Microstrip antenna design with improved fabrication tolerance for remote vital signs monitoring and WLAN/WPAN applications at mm-Wave and THz frequencies," Ph.D. dissertation, Dept. Electron. Electr. Syst. Eng., Univ. Birmingham, Birmingham, U.K., 2018.

SOLOMON MINGLE received the M.Sc. degree in communications engineering and networks from the University of Birmingham in 2019, where he currently pursuing the Ph.D. degree in wireless communications and sensors. He has developed unique leaky wave antennas and metamaterial antennas for emerging short-range broadband mobile communications in dynamic environments, as well as beam-steered Doppler radar-based remote health monitoring devices operating in the microwave and millimetre-wave range. He is currently a Ph.D. Researcher with the Department of Electronics, Electrical and Systems Engineering, University of Birmingham, where he is working on dielectric image lines and metamaterial-based frequency sensing antennas for future wireless sensors for health monitoring, IoT, and space applications in the millimetre-wave range. He has published more than six academic papers on antenna design and measurements for wireless technologies.

DESPOINA KAMPOURIDOU (Member, IEEE) was born in Greece, in 1990. She received the electrical and computer engineering degree from the Aristotle University of Thessaloniki, Greece, in 2015, and the Ph.D. degree in electrical, electronic and systems engineering from the University of Birmingham, U.K., in 2020.

Since 2019, she has been a Research Fellow with the Department of Electrical, Electronic and Systems Engineering, University of Birmingham. In 2020, she was awarded a Royal Academy of Engineering U.K. Intelligence Community Postdoctoral Research Fellowship from 2020 to 2022. Her research interests include analysis and design of metamaterials, leaky-wave antennas, dispersion analysis methods, and microwave circuits. She is the Technical Chamber of Greece.

ALEXANDROS FERESIDIS (Senior Member, IEEE) was born in Thessaloniki, Greece, in 1975. He received the physics degree from the Aristotle University of Thessaloniki, Greece, in 1997, the M.Sc. (Eng.) degree in radio communications and high frequency engineering from the University of Leeds, U.K., in 1998, and the Ph.D. degree in electronic and electrical engineering from Loughborough University, U.K., in 2002.

During the first half of 2002, he was a Research Associate and in the same year he was appointed as a Lecturer of Wireless Communications with the Department of Electronic and Electrical Engineering, Loughborough University, where, in 2006, he was promoted to Senior Lecturer. In December 2011, he joined the Department of Electronic, Electrical and Systems Engineering, University of Birmingham, U.K., where he is currently a Professor of Microwave and Terahertz Communications. He has published more than 190 papers in peer reviewed international journals and conference proceedings and has coauthored five book chapters. His research interests include analysis and design of metamaterials, electromagnetic band gap structures and frequency selective surfaces, leaky-wave antennas, small/compact antennas, passive microwave/mm-wave/THz circuits, microfabrication, numerical techniques for electromagnetics, and bioelectromagnetics.

Prof. Feresidis has held a Senior Research Fellowship Award from the U.K. Royal Academy of Engineering and The Leverhulme Trust from 2013 to 2014. He is a member of the U.K. EPSRC Peer Review College, he was on the editorial board of *IET Microwaves, Antennas and Propagation* journal from 2014 to 2018 and he is currently an Associate Editor in the IEEE TRANSACTIONS ON ANTENNAS AND PROPAGATION.